RSC Advances

PAPER

View Article Online
View Journal | View Issue

Cite this: *RSC Adv.*, 2020, **10**, 4064

Electrochemical heavy metal removal from water using PVC waste-derived N, S co-doped carbon materials†

Yingna Chang,‡[a] Qidong Dang,‡[b] Imran Samo,[a] Yaping Li,[a] Xuejin Li,[b] Guoxin Zhang *[b] and Zheng Chang *[a]

Received 7th November 2019
Accepted 26th December 2019

DOI: 10.1039/c9ra09237d

rsc.li/rsc-advances

The removal of heavy metal contaminants has aroused global attention due to water shortage and the lax control on the discharge of heavy metal pollutants. Capacitive deionization (CDI) has emerged as a robust, energy-/cost-efficient technique for water treatment. Herein, we reported the simple synthesis of N, S-co-doped carbon materials (NS-C) derived from PVC plastic wastes as CDI electrode materials for the efficient removal of heavy metal ions (HMIs). The NS-C exhibited a large specific surface area (~1230 $m^2\ g^{-1}$) and contained heavy heteroatom doping (~4.55 at% N and ~13.30 at% S). The CDI electrode fabricated using NS-C showed high removal efficiency (94–99%), high capacity (36–62 mg g^{-1}), and good regeneration capability for the adsorption of various kinds of low-concentration heavy metal ions (including Fe^{2+}, Co^{2+}, Ni^{2+}, Cu^{2+}, Pb^{2+}, and Cd^{2+}). Moreover, PVC plastic wastes that are heavily accumulated in the environment and extremely hard to be decomposed and recycled were applied as the carbon source in this study for the fabrication of NS-C, which further rendered the importance of our study in practically treating hazardous waste (HMIs) with waste (PVC plastic wastes) in a clean and efficient way.

1. Introduction

Currently, the issues of water pollution and scarcity have gained ever-growing global concern.[1–3] Heavy metal species (such as Fe^{2+}, Co^{2+}, Ni^{2+}, Cu^{2+}, Zn^{2+}, Pb^{2+}, and Cd^{2+}) are largely produced from the steel, electronics, and battery industries, and can be extremely hazardous to living beings.[4] In addition, the biodegradation of HMIs is difficult and they are more easily accumulated through agriculture and ground water paths relative to organic pollutants.[5] Therefore, HMIs urgently need to be removed down to permissible limits before being discharged into the environment. Currently, many techniques have been developed to tackle HMI pollutants in water, mainly including adsorption (with[6–8] or without[9] voltage applied), precipitation,[10,11] ion exchange,[12,13] reverse osmosis,[14,15] and membrane separation.[16] Among them, electric field-driven adsorption, *i.e.*, capacitive deionization (CDI), using a porous carbon electrode, such as activated carbon, can effectively remove HMIs from contaminated water (the applied voltages typically lie in the low voltage range of 0.8–1.4 V).[17–19] In addition, it holds ultrahigh efficiency for HMIs present in low concentrations (typically lower than 200 ppm)[20] and can quickly regenerate the electrode by simply releasing the outer applied voltage.[21] However, temporarily, electrode materials used for CDI either do not have a satisfying capacity (such as commercial activated carbon),[18,19,22] or are obtainable only with tedious procedures[23] and expensive precursors (such as graphene,[17,20,24] carbon nanotubes,[5,25] layered oxide/sulfide,[26,27] and Mxene[28]), which places considerable barriers for practical applications of CDI techniques.

Carbon-based electrode materials for CDI are promising options in terms of their wide availability at low costs.[2,3,22] In particular, many natural products, such as glucose,[29,30] sucrose,[31–33] and cellulose,[34,35] can be used as carbon sources to fabricate carbonaceous materials. In order to gain carbon materials with a higher adsorption capacity, it is applicable and feasible to involve heteroatom doping to provide more anchoring sites for metal ions.[36,37] Common strategies for incorporating heteroatom species into carbon materials are mainly based on the pyrolysis of organics that contain heteroatom sources. However, these inevitably generate hazardous volatile organic compounds and lead to uncontrollable doping types and contents.[37]

Recently, a simple and effective dehalogenation strategy for fabricating doped carbon materials under mild conditions was developed.[17,39–42,52–54] For instance, over 10 at% nitrogen can be

[a]*State Key Laboratory of Chemical Resource Engineering, Beijing University of Chemical Technology, Beijing, 100029, China. E-mail: changzheng@mail.buct.edu.cn*
[b]*College of Electrical Engineering and Automation, Shandong University of Science and Technology, Qingdao 266590, China. E-mail: zhanggx@sdust.edu.cn*

† Electronic supplementary information (ESI) available: The scheme of an integrated capacitive deionization apparatus; additional electron microscopy images of N-C, S-C, and NS-C; XRD profiles of N-C, S-C, and NS-C; supercapacitor characterizations of NS-C; CDI cycling stability measurements of NS-C. See DOI: 10.1039/c9ra09237d

‡ These authors contributed equally to this work.

incorporated into the as-formed carbon at room temperature under simple hand grinding.[17] The ultrahigh doping efficiency is mainly due to the high reactivity of dehalogenated carbon sites that are capable of fast coupling with adjacent atoms.[43] Polyvinyl chloride (PVC) is one sort of widely applicable halogenated polymer in daily life, but is extremely hard to decompose and recycle due to its extremely stable physico-chemical properties. Currently, the severe PVC accumulation has caused irreversible damage to our environment.[44–47] It is of significance and practicality to fabricate doped carbon materials from PVC and explore their CDI applications.

Here in this study, we managed to fabricate a N, S-co-doped carbon material (NS-C) by dehalogenating PVC plastic wastes using KOH in the presence of thiourea (N/S dopant). It was characterized that 4.55 at% N and 13.30 at% S were doped in the resulting NS-C. Meanwhile, the NS-C is highly porous and contains a multi-scale hierarchical pore (macro-/meso-/micropores), achieving a high specific surface area of 1230 $m^2\ g^{-1}$. The NS-C, once fabricated into the CDI electrode, exhibited very high removal efficiency (94–99%), high capacity (36–62 $mg\ g^{-1}$), and good regeneration performance towards capacitive adsorbing of various kinds of low concentration HMIs. CDI measurements showed that NS-C presented a larger affinity and capacity for HMIs over alkali metal ions and alkali earth metal ions due to the heavy heteroatom doping. Moreover, the dehalogenation route of applying PVC plastic wastes as a carbon source to synthesize CDI electrode materials may potentially open up clean, efficient disposal and prosperous utilization of annoying PVC plastic wastes, which is a worthwhile "kill two birds with one stone" strategy to control waste by waste.

2. Experimental section

2.1 Materials

A PVC waste document bag was obtained from the living garbage. Dimethylformide (DMF), dimethylsulfoxide (DMSO), thiourea, potassium hydroxide (KOH), hydrochloric acid (HCl), and various metal chlorides, including $FeCl_2$, $CoCl_2$, $NiCl_2$, $CuCl_2$, $PbCl_2$, or $CdCl_2$ were purchased from Beijing Chemical Works and Aladdin Chemistry Co., Ltd. All chemical reagents were used without further purification.

2.2 Preparation of N, S-co-doped carbon materials

1.0 g PVC wastes was dissolved in 10 mL DMF. Then, the dissolved PVC suspension, 2.0 g KOH and 1.0 g thiourea were added into a ZrO_2 ball mill jar. The mixture was ball-milled at 30 Hz for 2 h, and then dried at 60 °C overnight, and then annealed in a tubular furnace at 600 °C for 2 h under nitrogen protection with a heating rate of 10 °C min^{-1}, resulting in a black solid. Finally, the product was washed with 5% HCl and purified with distilled water at least 3 times, followed by drying. The as-obtained N, S-co-doped carbon was labelled as NS-C. To compare the effects of S and N, DMSO and DMF were used as dopants to replace the thiourea for S and N doping in the above process, and the resulting samples were correspondingly named as S-C and N-C.

2.3 Characterizations

The morphologies and crystal structures of the NS-DCM were studied by scanning electron microscopy (SEM, Zeiss SUPRA55), transmission electron microscopy (TEM, JEOL JEM-2100), powder X-ray diffraction (XRD, Shimadzu XRD-6000) and Raman spectroscopy (HORIBA Jobin Yvon). X-ray photoelectron spectroscopy (XPS) was performed on a Thermo Electron ESCALAB 250 XPS spectrometer. The N_2 adsorption/desorption isotherms were examined by a Quantachrome Adsorption Instrument (Quantachrome Autosorb-1CVP). The specific surface area was calculated from the adsorption branch according to the Brunauer–Emmett–Teller (BET) method. The pore size distribution plot was derived from the adsorption branch of the isotherm based on the Barrett–Joyner–Halenda (BJH) method.

2.4 Electrochemical measurements

The electrochemical performance of materials was examined by the CHI 660E electrochemical workstation (Shanghai, Chenhua) with a three-electrode setup. The cyclic voltammetry (CV), electrochemical impedance spectroscopy (EIS), and galvanostatic charge–discharge (GCD) were carried out in Na_2SO_4 (1.0 mol L^{-1}) solutions.

2.5 Capacitive deionization (CDI) experiment

The CDI electrode was prepared by loading 100 mg mixture of NS-C, acetylene black, and 5.0 wt% PTFE with a mass ratio of 80 : 15 : 5 in 2.0 mL ethanol and thoroughly sonicating to reach a homogenous slurry. Then, the viscous slurry was uniformly coated on a graphite paper (size: 6.0 cm × 7.0 cm × 0.2 mm) and dried in an oven at 80 °C overnight. In a typical CDI measurement, 100.0 mL aqueous solution with an initial metal ion concentration of 50 ppm ($FeCl_2$, $CoCl_2$, $NiCl_2$, $CuCl_2$, $PbCl_2$, or $CdCl_2$) in a beaker was continuously fed into the CDI unit using a peristaltic pump with a constant flow rate of 25.0 mL min^{-1} and the effluent was returned to the beaker. Meanwhile, the applied voltage was 1.5 V for adsorption and −1.5 V for desorption. The concentration of solution was monitored by a conductivity meter (Type 308F, Leici Company) located at the outlet of the CDI unit (as schemed in Fig. S1†). As shown in Fig. S2,† there is a linear relationship between the conductivity of the solution and the concentration of metal ions. In order to measure the selectivity, a 100.0 mL mixture solution containing 20 ppm Mg^{2+}, 20 ppm Ni^{2+}, and 20 ppm Pb^{2+} was used. After CDI treatment, the final concentrations of three metal ions were measured by an inductively coupled plasma-atomic emission spectrometer (Thermo, ICP-6300).

The adsorption capacity of heavy metals (W) was calculated by the following eqn (1):

$$W = \frac{(C_0 - C) \times V}{m} \quad (1)$$

where C_0 and C are the initial and final concentrations, respectively, and V is the total volume of the solution and m is the mass of the electrode carbon materials. The ion

accumulated removal rate (U) was calculated according to the following eqn (2):

$$U = \frac{W}{t} \quad (2)$$

where t is working time. The removal efficiency (Y) was calculated by the following eqn (3):

$$Y = \frac{C_0 - C}{C_0} \quad (3)$$

3. Results and discussion

As schematically represented in Fig. 1A, the fabrication of NS-C involved two main steps: (1) ball milling PVC fragments (hand-cut), KOH, and thiourea (N, S dopant) in DMF (the resulted carbonaceous material was named as RT-NS-C); (2) annealing the RT-NS-C precursor at 600 °C (resulted carbon material was named as NS-C). Annealing was applied to gain conductivity and stabilize the doped heteroatom.[37,48] As revealed by the dark black colour of RT-NS-C, it is evident that the defunctionalization and carbonization of PVC could be promoted by KOH at room temperature, which was similar to that of PVDC.[38] RT-NS-C without water washing was examined by TEM (Fig. S3A†), revealing the presence of cube-shaped crystals as well as an amorphous matrix (carbonaceous materials were obtained from the dehalogenation of PVC by KOH). Further XRD characterization (Fig. S3B†) confirmed that these nanocubes were KCl, which were generated from the reaction of PVC and KOH.[49] After annealing and washing, the NS-C and the control samples (N-C and S-C) were examined by electron microscopy (Fig. 1B/C and S4A/B†), indicating that they possessed obvious open porous structures. These open pores probably resulted from the bubbling effects of gaseous products like CO, CO_2, NO_2, SO_2 during the annealing with KOH assistance.[36,48] XRD measurements revealed that the phases of the as-synthesized doped carbon materials after water washing were amorphous (Fig. 2A), which agreed with previous reports about synthetic carbon materials.[37] Organic elemental analysis (OEA) was performed in order to measure the elemental contents. Fig. 1D shows that NS-C contained 66.1 at% C, 10.0 at% O, 4.6 at% N, 13.3 at% S, and 1.0 at% H. In contrast, the control samples of N-C and S-C contained 5.0 at% N and 5.8 at% S, respectively. Therefore, applying thiourea as the N, S dopant was key for achieving a high dopant content.

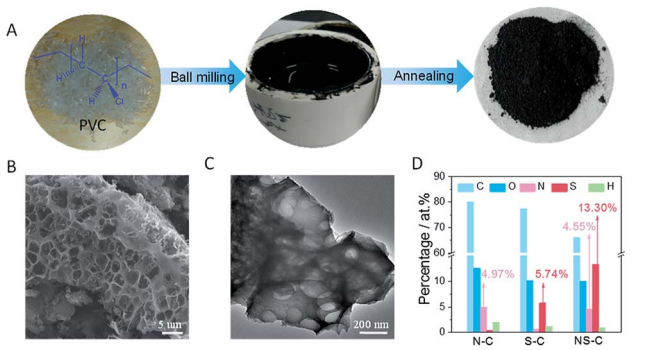

Fig. 1 (A) Fabrication scheme for NS-C from PVC plastic waste. (B) SEM and (C) TEM images of PVC-derived NS-C. (D) Organic elemental analysis of N-C, S-C, and NS-C.

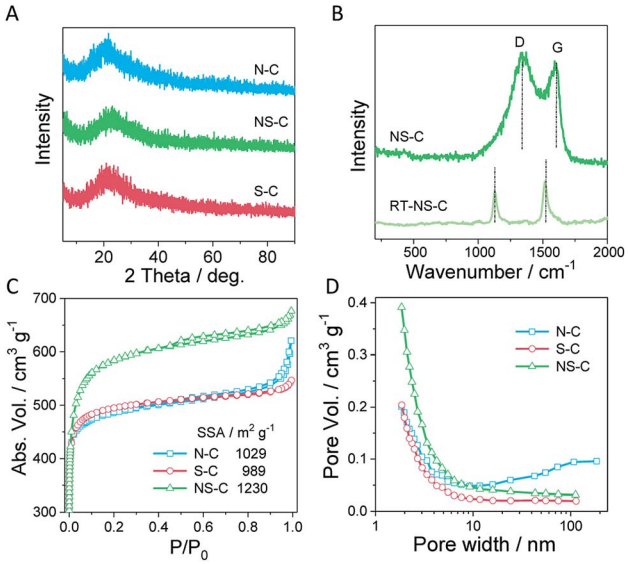

Fig. 2 (A) XRD spectra and (B) Raman spectra of RT-NS-C and NS-C. (C) N_2 absorption/desorption curves and (D) pore size distribution curves of N-C, S-C, and NS-C.

As revealed in Fig. 2B, there were two distinct Raman bands presented for both RT-NS-C and NS-C. The bands of NS-C located at ~1346 and ~1604 cm^{-1} could be unambiguously indexed to the D and G bands for graphitic carbon materials, respectively.[50] Meanwhile, RT-NS-C exhibited a set of bands consisting of two sharp bands but the bands were heavily blue-shifted to ~1127 and ~1519 cm^{-1}, confirming that RT-NS-C is highly carbonized.[43] The pore type of NS-C, as revealed by N_2 adsorption/desorption curves (Fig. 2C), could be indexed to a combination of type-I and type-II pores, which suggests that huge amounts of micropores and a small proportion of mesopores and macropores exist.[38] Due to similar protocols, the control samples of N-C and S-C exhibited similar N_2 adsorption/desorption curves. The specific surface areas (SSA) of NS-C, N-C, and S-C were 1230, 1029, and 989 $m^2\ g^{-1}$, respectively. Fig. 2D displays their pore distribution curves, revealing the overwhelmingly present micropores in all three samples. The minor amount of mesopores ($\Phi \sim 2$–10 nm) were mainly introduced by the rapid removal of gas bubbles and KOH activation.[48]

XPS measurements were employed to characterize the surface composition of NS-C. There were mainly four types of elements present in NS-C: carbon (C 1s, ~285 eV), oxygen (O 1s, ~532 eV), nitrogen (N 1s, ~400 eV), and sulphur (S 2p, ~164 eV), as shown in Fig. 3A. Deconvolution was performed on each element for detailed bond configurations. In the C 1s spectra (Fig. 3B), it was revealed that over 25.6% carbon atoms were connected to non-carbon atoms, including O, N and S, which is further evidenced by the ultrahigh content of heterodoped elements. As shown in the S 2p spectra (Fig. 3D), S and C

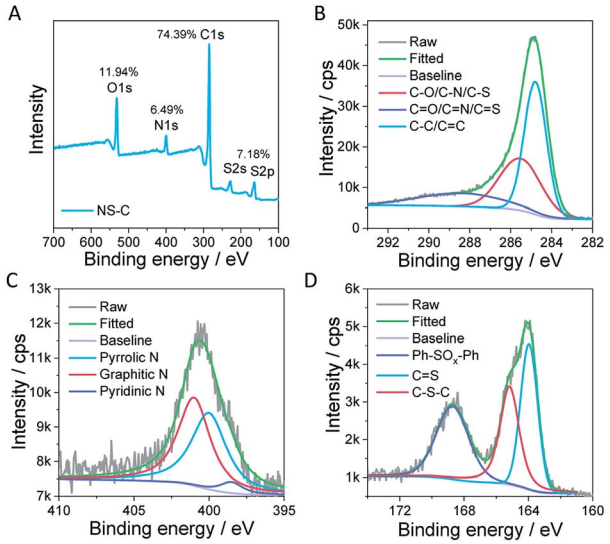

Fig. 3 (A) The XPS survey, (B) C 1s, (C) N 1s, and (D) S 2p XPS spectra of NS-C and their deconvoluted curves.

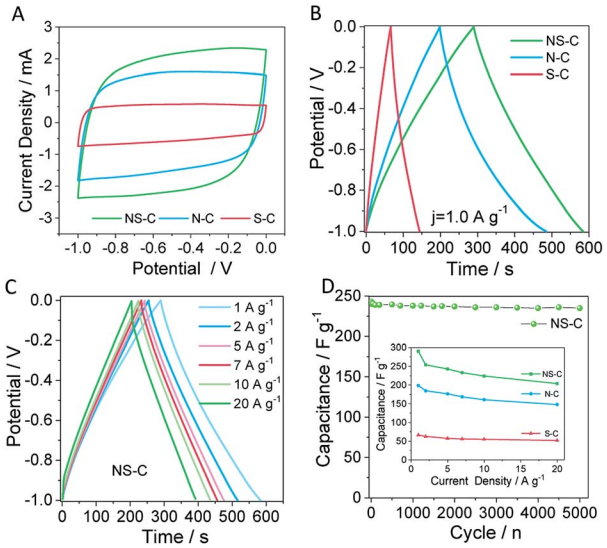

Fig. 4 Supercapacitor measurements of NS-C/N-C/S-C in 1.0 M Na_2SO_4. (A) CV profiles at scan rate of 100 mV s^{-1}, (B) charge/discharge curves at 1.0 A g^{-1}, (C) charge/discharge curves of NS-C at different current, (D) cycling stability of NS-C, inset shows the capacitances of NS-C/N-C/S-C at different rates.

connections could be sorted into three types: C–S single bond, C═S double bond, and oxidized S bound to C. The considerable amount of oxidized S in the carbon matrix was probably due to the KOH activation and oxidation during the high-temperature treatment. N 1s spectra (Fig. 3C) indicated that the N species mainly existed in a pyrrolic and graphitic N forms, accompanied by negligible amount of pyridinic N. The ultrahigh content of alien species was further confirmed by organic elemental analysis, reaching 27.8 at% (combining O, N, and S), which provided abundant sites for anchoring metal cations.

Therefore, the as-made samples were fabricated into electrodes for supercapacitor measurements in aqueous Na_2SO_4 solution (1.0 mol L^{-1}) prior to the CDI tests. As shown in Fig. 4A and S5A–C,† all the CV profiles of the as-obtained materials exhibited a near-rectangular shape, suggesting that the electrochemical double-layer capacitive behaviour dominated all three samples. Among them, the NS-C showed the largest area, meaning more charge was capable of being stored in NS-C than in N-C and S-C, which was possibly due to its higher degree of doping and synergistic effect of dual N, S doping.[48] As measured by galvanic charge/discharge (Fig. 4B and S5D/E†), the NS-C sample delivered a very high capacitance of 290.2 F g^{-1} (at 1.0 A g^{-1}) in Na_2SO_4 aqueous solutions, which is superior to that of N-C and S-C. Remarkably, the NS-C was able to maintain over 70.3% of capacitance during charge/discharge at a high rate of 20.0 A g^{-1} (Fig. 4C and inset of Fig. 4D). As shown in Fig. 4D, over 96.7% capacitance of the NS-C could be kept after high-rate cycling for 5000 times at a current density of 5.0 A g^{-1}, implying that the NS-C was electrochemically stable under the measurement conditions in a concentrated alkaline solution. All in all, we managed to exploit the supercapacitor application of PVC waste-rendered porous N, S-co-doped carbon materials.

Furthermore, the NS-C material, having a large SSA, open porous structure, high-content heteroatom doping, and large specific capacitance, was submitted to HMI removal tests using a bench-scale capacitive deionization (CDI) apparatus consisting of a pump, a conductivity meter, an electrical power supply, a self-made CDI unit, and a feed water reservoir (Fig. S1†). The conductivity change is closely related to the ion concentration in solution, which helps in monitoring the adsorption/desorption processes of ions.[36] Normally, single-element doping in carbon materials such as N or S provides robust sites for ions to anchor. Herein, the as-fabricated NS-C provided much more heteroatom doping sites than single N or S doped carbon materials, as shown in Fig. 1D. Initially, a voltage was not applied to reveal the extent of physical adsorption. It was observed that the system conductivity exhibited a negligible

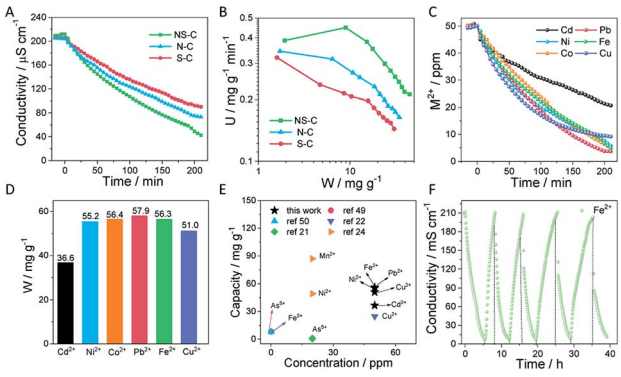

Fig. 5 Capacitive deionization behaviours at 1.5 V. (A) Deionization curves for Fe^{2+} in 50 ppm aqueous $FeCl_2$ solution, and (B) plots of removal rate *versus* capacity for N-C/S-C/NS-C. (C) Deionization curves, and (D) capacities in various heavy metal ion solutions (50 ppm). (E) Comparison with state-of-the-art electrode materials for the removal of HMI, and (F) cycling stability of NS-C for the removal and release of Fe^{2+}.

conductivity decrease in the first 20 min (Fig. 5A), meaning that the physical adsorption with the circumstance of no applied voltage was not prominent. Upon voltage was applied, the conductivity for each testing system was observed to sharply drop. The comparison of the deionization curves of NS-C and two control samples (N-C and S-C) for Fe^{2+} is displayed in Fig. 5A/B. It was confirmed that the co-doped carbon materials (NS-C) exhibited a superior deionization capacity and faster deionization rates than that of the other samples with single-element doping. The significant improvement of NS-C in the removal of HMIs could be attributed to the large accessible SSA and deeply activated carbon surface by the introduction of rich heteroatom doping sites.

The standard curves of conductivity *versus* concentration for different metal ions are plotted in Fig. 5C. The applied voltage (1.5 V) was used in the adsorption process and the voltage was reversed (−1.5 V) in the desorption process. Due to the difficulty in treating low-concentration HMIs, the deionization performance was investigated in 50 ppm HMI solutions including Fe^{2+}, Co^{2+}, Ni^{2+}, Cu^{2+}, Pb^{2+}, and Cd^{2+}. Prior to all CDI measurements, we first recorded the pH variations of a 50 ppm Fe^{2+} solution during the CDI measurements in Fig. S6.† The initial pH of the solution was ~5.75 and along with the CDI process of absorbing Fe^{2+}, the pH value gradually increased to 6.23 at the end of the CDI, suggesting that the pH had limited fluctuation. Meanwhile, there was no obvious redox peak of NS-C in the 50 ppm Fe^{2+} solution under a scan rate of 5 mV s^{-1} (Fig. S7†), implying a dominating electrochemical double-layer capacitive behaviour against faradic reactions. Upon the voltage was applied, it was forced to reach a close-to-zero conductivity threshold for the cases of Cu^{2+}, Pb^{2+} and Ni^{2+} over 210 min (Fig. 5C). The final ion concentrations calculated from the corresponding conductivity at 210 min were reduced to 5.8, 3.7, and 9.2 ppm for Ni^{2+}, Pb^{2+}, and Cu^{2+} from 50 ppm, respectively. The removal capacities for Fe^{2+}, Co^{2+}, Ni^{2+}, Cu^{2+}, Pb^{2+} and Cd^{2+} as calculated from deionization curves were 56.3, 56.4, 55.2, 51.0, 57.9 and 36.6 mg g^{-1}, respectively (Fig. 5D). The significance in the adsorption rate constants for different cations may arise from their different affinity with heterodoping atoms.[17,20,22] Such high removal capacities for various heavy metal cations surpassed most current reported values applying CDI techniques (Fig. 5E).[17,22,49–51]

The regeneration capability of CDI electrode materials is another important aspect for practical applications. Capacities and efficiencies of deionizing heavy metal ions after the adsorption equilibrium using the NS-C electrode in different cycles were investigated and recorded. As shown in Fig. 5F and S8,† over five consecutive adsorption/desorption cycles for 50 ppm Fe^{2+} revealed that the system conductivity was recoverable with voltage converting and the deionization efficiency for all cycles was above 99%, indicating a high efficiency and remarkable stability of the NS-C electrode, which was probably related to the negligible physical adsorption.

We further explored the capability of NS-C to selectively adsorb HMIs over low toxicity metal ions in a mixed solution. Fig. S9† shows the deionization curve of NS-C using a CDI system in a mixed ionic solution containing 20 ppm Mg^{2+}, 20 ppm Ni^{2+}, and 20 ppm Pb^{2+}. While being monitored, the conductivity of the mixed solution took a sharp decrease in the first 60 min and finally reached a plateau. For exactly measuring the removed ions, the mixed solutions were submitted to ICP measurements before and after the CDI process at 210 min. Though the starting concentrations for each type of ion were all 20 ppm, after CDI, it was exciting to find that nearly all HMIs had been removed from the mixed solution while only ~6.7 ppm Mg^{2+} was left. Therefore, NS-C held a larger affinity and capacity for HMIs over less hazardous alkali metal ions and alkali earth metal ions, which might be attributed to the huge amount of cooperative heteroatom doping in the electrode materials. For a real CDI system, it is not possible to completely remove all the ions in solution. However, there is a significant difference in the achievable adsorption thresholds when using different electrode materials. As is well known, the removal of very low concentrations of HMIs is still a challenge. Herein, the concentration of Co^{2+} decreased to 1 ppm to study the removal capacity of NS-C electrode materials using the CDI technique. As shown in Fig. S10,† the removal efficiency rapidly reached 57.8% in 30 min and finally 82.6% in equilibrium.

4. Conclusions

In conclusion, heavily N, S-co-doped carbon material (NS-C) was fabricated *via in situ* doping the dehalogenated sites of PVC with thiourea (common plastic waste was used as the PVC source). It was revealed that, in contrast to the usage of single-element dopants, thiourea engaged more foreign atoms into the carbon matrix, resulting in ultrahigh doping levels of ~4.55 at% N and ~13.30 at% S. Meanwhile, the NS-C was highly porous and afforded a very high SSA of 1230 m^2 g^{-1}. The NS-C-fabricated CDI electrode exhibited high adsorption capacities for many HMIs, including Fe^{2+} (56.3 mg g^{-1}), Co^{2+} (56.4 mg g^{-1}), Ni^{2+} (55.2 mg g^{-1}), Cu^{2+} (51.0 mg g^{-1}), Pb^{2+} (57.9 mg g^{-1}), and Cd^{2+} (36.6 mg g^{-1}), respectively in 50 ppm heavy metal ions solutions. Meanwhile, the NS-C electrode achieved high removal efficiencies (94–99%) and good regeneration performance towards adsorbing various kinds of heavy metals ions, especially Fe^{2+}. In addition, it was confirmed that the NS-C had a larger affinity and capacity for HMIs over less hazardous alkali metal ions and alkali earth metal ions, which was one efficient way to make full use of NS-C materials. Our work may potentially open up "one-stone-two-bird" sustainable reuse of PVC wastes that are heavily accumulated in our environment and convert them into value-added functional carbon materials as superior electrode materials for supercapacitor and CDI applications.

Conflicts of interest

There are no conflicts to declare.

Acknowledgements

This work was financially supported by the National Natural Science Foundation of China (NSFC, 21471014 and 21701101),

the Program for Changjiang Scholars and Innovation Research Team in the University, the National Key Research and Development Project (2016YFF0204402), the Shandong Scientific Research Awards Foundation for Outstanding Young Scientists (ZR2018JL010), the Shandong Joint Fund of Outstanding Young Talents (ZR2017BB018), and the Fundamental Research Funds for the Central Universities. We also thank the Scientific Research Foundation of Shandong University of Science and Technology for Recruited Talents (2017RCJJ059), and Key Research and Development Plan of Shandong Province (2019GGX103032).

References

1 Y. Oren, *Desalination*, 2008, **228**, 10–29.
2 V. K. Gupta and T. A. Saleh, *Environ. Sci. Pollut. Res.*, 2013, **20**, 2828–2843.
3 S. Porada, R. Zhao, A. van der Wal, V. Presser and P. M. Biesheuvel, *Prog. Mater. Sci.*, 2013, **58**, 1388–1442.
4 Q. Liao, W. Pan, D. Zou, R. Shen, G. Sheng, X. Li, Y. Zhu, L. Dong, A. M. Asiri, K. A. Alamry and W. Linghu, *J. Mol. Liq.*, 2018, **261**, 32–40.
5 D. K. Yadav and S. Srivastava, *Mater. Today: Proc.*, 2017, **4**, 4089–4094.
6 M. S. Gaikwad and C. Balomajumder, *Sep. Purif. Technol.*, 2017, **195**, 305–313.
7 Z. Li, J. Chen, H. Guo, X. Fan, Z. Wen, M. Yeh, C. Yu, X. Cao and Z. Wang, *Adv. Mater.*, 2016, **28**, 2983–2991.
8 J. Wang, J. Li and J. Wei, *J. Mater. Chem. A*, 2015, **3**, 18163–18170.
9 P. Drogui, N. Meunier, G. Mercier and J. F. Blais, *Int. J. Environ. Waste Manage.*, 2011, **8**, 241–257.
10 N. Meunier, P. Drogui, C. Montané, R. Hausler, G. Mercier and J. F. Blais, *J. Hazard. Mater.*, 2006, **137**, 581–590.
11 C. H. Huang, L. Chen and C. L. Yang, *Sep. Purif. Technol.*, 2009, **65**, 137–146.
12 Z. Wang, Y. Feng, X. Hao, W. Huang and X. Feng, *J. Mater. Chem. A*, 2014, **2**, 10263–10272.
13 Z. Wang, S. Guo, Z. Wu, H. Fan, G. Guan and X. Hao, *Sep. Purif. Technol.*, 2017, **187**, 199–206.
14 L. Lin, X. Xu, C. Papelis, T. Y. Cath and P. Xu, *Sep. Purif. Technol.*, 2014, **134**, 37–45.
15 S. H. Joo and B. Tansel, *J. Environ. Manage.*, 2015, **150**, 322–335.
16 Y. Peng, H. Huang, Y. Zhang, C. Kang, S. Chen, L. Song, D. Liu and C. Zhong, *Nat. Commun.*, 2018, **9**, 187.
17 P. Liu, T. Yan, J. Zhang, L. Shi and D. Zhang, *J. Mater. Chem. A*, 2017, **5**, 14748–14757.
18 L. Yong, L. Pan, T. Chen, X. Xu, T. Lu, S. Zhuo and D. H. C. Chua, *Electrochim. Acta*, 2015, **151**, 489–496.
19 A. M. Dehkhoda, N. Ellis and E. Gyenge, *Microporous Mesoporous Mater.*, 2016, **224**, 217–228.
20 L. Liu, X. Guo, R. Tallon, X. Huang and J. Chen, *Chem. Commun.*, 2016, **53**, 881–884.
21 C. S. Fan, S. C. Tseng, K. C. Li and C. H. Hou, *J. Hazard. Mater.*, 2016, **312**, 208–215.
22 S. Y. Huang, C. S. Fan and C. H. Hou, *J. Hazard. Mater.*, 2014, **278**, 8–15.
23 M. M. Chen, D. Wei, W. Chu, T. Wang and D. G. Tong, *J. Mater. Chem. A*, 2017, **5**, 17029–17039.
24 X. Gu, Y. Yang, Y. Hu, M. Hu and C. Wang, *ACS Sustainable Chem. Eng.*, 2015, **3**, 1056–1065.
25 Z. Sui, Q. Meng, X. Zhang, R. Ma and B. Cao, *J. Mater. Chem.*, 2012, **22**, 8767–8771.
26 D. Sarma, S. M. Islam, K. S. Subrahmanyam and M. G. Kanatzidis, *J. Mater. Chem. A*, 2016, **4**, 16597–16605.
27 Q. Peng, L. Liu, Y. Luo, Y. Zhang, W. Tan, F. Liu, S. L. Suib and G. Qiu, *ACS Appl. Mater. Interfaces*, 2016, **8**, 34405–34413.
28 W. Bao, X. Tang, X. Guo, S. Choi, C. Wang, Y. Gogotsi and G. Wang, *Joule*, 2018, **2**, 778–787.
29 X. Sun and Y. Li, *Angew. Chem., Int. Ed.*, 2004, **43**, 597–601.
30 S. Ikeda, K. Tachi, Y. Hau Ng, Y. Ikoma, T. Sakata, H. Mori, A. Takashi Harada and M. Matsumura, *Chem. Mater.*, 2007, **19**, 4335–4340.
31 K. Böhme, W. D. Einicke and O. Klepel, *Carbon*, 2005, **43**, 1918–1925.
32 D. L. Sivadas, S. Vijayan, R. Rajeev, K. N. Ninan and K. Prabhakaran, *Carbon*, 2016, **109**, 7–18.
33 L. Shi, Y. Chen, H. Song, A. Li, X. Chen, J. Zhou and Z. Ma, *Electrochim. Acta*, 2017, **231**, 153–161.
34 X. Tian, S. Zhu, J. Peng, Y. Zuo, G. Wang, X. Guo, N. Zhao, Y. Ma and L. Ma, *Electrochim. Acta*, 2017, **241**, 170–178.
35 L. Jiang, G. W. Nelson, S. O. Han, H. Kim, I. N. Sim and J. S. Foord, *Electrochim. Acta*, 2016, **192**, 251–258.
36 L. Chao, Z. Liu, G. Zhang, X. Song, X. Lei, M. Noyong, U. Simon, Z. Chang and X. Sun, *J. Mater. Chem. A*, 2015, **3**, 12730–12737.
37 Q. Wang, Y. Ji, Y. Lei, Y. Wang, Y. Wang, Y. Li and S. Wang, *ACS Energy Lett.*, 2016, **3**, 1183–1191.
38 Z. Liu, G. Zhang, Z. Lu, X. Jin, Z. Chang and X. Sun, *Nano Res.*, 2013, **6**, 293–301.
39 G. Zhang, K. Zhou, R. Xu, H. Chen, X. Ma, B. Zhang, Z. Chang and X. Sun, *Carbon*, 2016, **96**, 1022–1027.
40 G. Zhang, J. Wang, B. Qin, X. Jin, L. Wang, Y. Li and X. Sun, *Carbon*, 2017, **115**, 28–33.
41 L. Cui, X. Wang, N. Chen, B. Ji and L. Qu, *Nanoscale*, 2017, **9**, 9089–9094.
42 D. Glas, J. Hulsbosch, P. Dubois, K. Binnemans and D. E. De Vos, *ChemSusChem*, 2014, **7**, 610–617.
43 J. Choi, H. Lee and S. Hong, *Desalination*, 2016, **400**, 38–46.
44 T. Zhao, Q. Zhou, X.-L. He, S.-D. Wei, L. Wang, J. M. N. van Kasteren and Y.-Z. Wang, *Green Chem.*, 2010, **12**, 1062–1065.
45 G. Zhang, H. Luo, H. Li, L. Wang, B. Han, H. Zhang, Y. Li, Z. Chang, Y. Kuang and X. Sun, *Nano Energy*, 2016, **26**, 241–247.
46 Y. Chang, G. Zhang, B. Han, H. Li, C. Hu, Y. Pang, Z. Chang and X. Sun, *ACS Appl. Mater. Interfaces*, 2017, **9**, 29753–29759.
47 M. Guo, C. Qiu, Y. Li, X. Jin, G. Zhang and X. Sun, *ChemElectroChem*, 2018, **5**, 242–246.
48 L. Yan, D. Li, T. Yan, G. Chen, L. Shi, Z. An and D. Zhang, *ACS Sustainable Chem. Eng.*, 2018, **6**, 5265–5272.

49 Z. Huang, L. Lu, Z. Cai and Z. J. Ren, *J. Hazard. Mater.*, 2015, **302**, 323.
50 L. Peng, Y. Chen, H. Dong, Q. Zeng, H. Song, L. Chai and J. D. Gu, *Water, Air, Soil Pollut.*, 2015, **226**, 1–11.
51 H. Li, L. Zou, L. Pan and Z. Sun, *Sep. Purif. Technol.*, 2010, **75**, 8–14.
52 Y. V. Kaneti, S. Dutta, M. S. Hossain, M. J. Shiddiky, K. L. Tung, F. K. Shieh, C. K. Tsung, K. C. W. Wu and Y. Yamauchi, *Adv. Mater.*, 2017, **29**, 1700213.
53 J. Kim, C. Young, J. Lee, M.-S. Park, M. Shahabuddin, Y. Yamauchi and J. H. Kim, *Chem. Commun.*, 2016, **52**, 13016–13019.
54 J. Tang, R. R. Salunkhe, H. Zhang, V. Malgras, T. Ahamad, S. M. Alshehri, N. Kobayashi, S. Tominaka, Y. Ide and J. H. Kim, *Sci. Rep.*, 2016, **6**, 30295.